JOURNAL OF CATALYSIS 127, 178–189 (1991)

Metal Deposition in Porous Anodic Alumina Films under Hydrotreating Conditions

N. NOURBAKHSH,* B. J. SMITH,†,[1] I. A. WEBSTER,‡,[2,3] J. WEI,† AND T. T. TSOTSIS*

University of Southern California, Department of Chemical Engineering, Los Angeles, California 90089-1211, †Massachusetts Institute of Technology, Department of Chemical Engineering, Cambridge, Massachusetts 02139; and ‡Unocal Science and Technology Division, UNOCAL CORPORATION, P. O. Box 76, Brea, California 92621

Received December 28, 1989; revised June 12, 1990

This work describes the condition of anodic alumina films aged during nickel etio-porphyrin hydrodemetallation. The films were examined in cross section by Transmission Electron Microscopy (TEM) and were depth profiled by X-ray Photoelectron Spectroscopy (XPS). The use of anodic alumina films with ideal porous structures allows examination by TEM of the mode of metal deposition inside single pores. TEM micrographs provide strong evidence of Ni present in the form of relatively large discrete crystallites rather than as a uniform layer on the pore walls as well as many other structural details impossible to extract from the examination of aged conventional alumina catalyst supports. © 1991 Academic Press, Inc.

1. INTRODUCTION

Residuum hydroprocessing catalysts consist of transition metal sulfides, typically Mo or W promoted with Co or Ni, dispersed on a high surface area support, usually Al_2O_3. During hydrodemetallation metals from the residuum feedstocks are deposited on the catalysts as metal sulfides. Hydroprocessing catalysts typically accumulate large amounts of contaminants during their working life. Of these contaminants metal deposits have been found to increase steadily with time on stream. Carbonaceous deposits on the catalyst build up rapidly to a steady-state level. The working form of the hydrodemetallation catalyst thus results from a complex interplay between the original catalytic materials (Co, Mo, and Al_2O_3) and the deposited or incorporated components (Ni, V, C, S, N, and Al_2O_3).

It has been postulated that metal sulfides accumulate in a uniform manner at the microscopic scale, building up layer by layer and effectively blocking access to the surface of the catalyst (*1, 2*). The model of microscopically uniform metal deposition has not been demonstrated by direct examination of the catalyst surface. Experimental results and models of nonuniform metal deposition have been reported (*3–5*). There is direct microscopic evidence from Transmission Electron Microscopy (TEM), as well as indirect spectroscopic evidence, that Ni and V sulfides deposit on HDM catalysts as large, spatially dispersed crystallites.

The objective of this work is to use anodically prepared alumina films, with an ideal porous structure, to obtain (by TEM) a visual picture of the metal deposition phenomena along the length of a single pore. These results are compared with those for a microporous γ-Al_2O_3 catalyst support, with low promoter levels. We have previously described the use of low surface area porous anodic alumina films in the study of catalyst deactivation during heavy Arabian residuum hydrotreating (*6*). In this study we use as an HDM reactant nickel etio-porphyrin

[1] Presently with Chevron Research Technology Company, 100 Chevron Way, P. O. Box 1627, Richmond, California 94802-0627.

[2] Presently with Unocal Corporate Division, Environmental Engineering Sciences, 1201 West 5th Street, P. O. Box 7600, Los Angeles, California 90051.

[3] To whom correspondence should be addressed.

0021-9517/91 $3.00

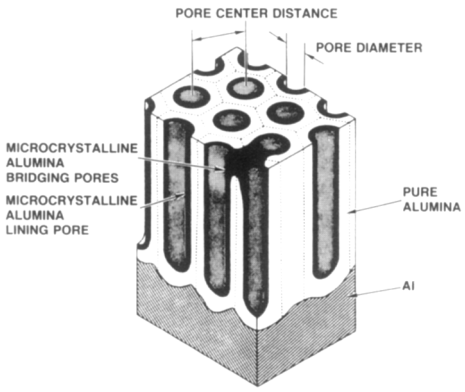

FIG. 1. Idealized porous type anodic oxide structure (*7*).

(Ni-EP), which is representative of the porphyrinic species present in heavy residua. TEM is used to obtain a visual picture of pore blockage and to identify the deposited crystallites within the pores.

2. EXPERIMENTAL

Alumina Support Preparation

The porous model alumina supports used in this study consist of thin layers of porous anodic alumina films, unpromoted except by residual *P* from the anodic preparation procedure, on an Al substrate. Their idealized structure is shown in Fig. 1.

They were prepared by anodizing pure Al discs ($\frac{1}{2}$ in. diameter, International Foils, Placentia, CA), in an electrochemical cell, using graphite cathodes (Princeton Applied Research, NJ). The electrolytes were prepared from analytical grade reagents (Baker) and distilled water. Electrolyte recirculation was achieved via an external peristaltic pump. In order to obtain films with pore sizes of 1000 Å, Al discs were anodized at 90 V for 1 h in a 0.4 *M* H_3PO_4 electrolyte at room temperature. This produced a 1.5-μm-thick porous film. At the conclusion of the anodization process, samples were thoroughly washed with distilled water and stored until the aging experiment.

In addition to the sample described above a microporous γ-Al_2O_3 sample with low promoter levels (American Cyanamid, Stamford, CT) was used for comparative studies. The physical properties of all the catalysts used in this study are summarized in Table 1. Industrial hydrotreating catalysts are typically characterized by a bimodal pore size distribution, with macropore diameters up to 1000 Å and micropore diameters of around 100 Å. The catalyst support used in this study has a unimodal pore size distribution, with a mean pore diameter of 85 Å.

Hydrodemetallation

The model compound used in this investigation was nickel etio-porphyrin (Ni-EP, Midcentury Chemicals, Posen, IL). The etio-porphyrin is believed to be representative of the porphyrinic species found in crude oils, which typically contain 10–15% of the metals. This porphyrin has been previously used by the MIT group in their HDM studies (*5, 8–11*).

Squalane (2,6,10,15,19,23-Hexamethyltetracosane, Sigma Chemical Co., St. Louis, MO), an isoparaffin, was used as the liquid carrier since it is free of S, N, and metal compounds, has a relatively high boiling point, a negligible vapor pressure at reaction conditions, and yet is a liquid at room temperature.

The experiments were carried out in a 2 liter stirred autoclave. The reactor system is described fully by Limbach (*12*) and Smith

TABLE 1

Samples Used in this Study

Sample no.	Material	Physical properties
1,2	γ-Al_2O_3 with low levels of Ni, Co, and Mo promoter.	Particle size of 75–88 μm, 258 m^2/g, pore diameter of 85 Å, 0.68 wt% Co, 0.32 wt% Ni, 0.25 wt% Si, 0.18 wt% P, and 0.24 wt% Mo.
3,4	Anodic alumina film, grown in 0.4 *M* H_3PO_4 electrolyte at 90 V for 1 h.	1.5-μm-thick film, 1000 Å pore diameter, 5 m^2/g, 1.8 g/cm^3, 3.4 wt% P, pore density of 30 pores/μm^2.

(*13*). The model alumina supports (Sample 4) and 3.1 g of a low promoter microporous γ-Al_2O_3 (Sample 2) were aged simultaneously in a series of eight batch HDM experiments. The microporous γ-Al_2O_3 powder was slurried in approximately 550 g of squalane in the stirred autoclave. Eight planar pieces of the model alumina support, each about 0.8 cm^2, were held in four baskets fixed to the bottom of the autoclave impeller, which was rotated at 1500 rpm. The total surface area of the microporous γ-Al_2O_3 powder was more than 1000 times that of the model alumina supports. So the observed HDM reaction rates are due to the catalytic effect of the microporous γ-Al_2O_3 support. Separate experiments confirmed that thermal reactions are not significant. To ensure consistency with other experiments conducted with CoMo/γ-Al_2O_3 catalysts, the alumina samples were presulfided. The sulfiding consisted of drying the catalyst at 110°C under a flow of He. The sulfiding was achieved with a mixture of 10 mol% H_2S/H_2 flowing at a rate of 100 cc/min. The temperature was held at 175°C for 6 h, raised to the final temperature of 315°C at a rate of 60°C/h, then maintained at this temperature for 1 h.

Each batch HDM experiment was initiated by cooling the reactor to 60°C. A concentrated slurry of Ni-EP in squalane was then added to the reactor to provide a starting Ni-EP concentration of 200 ppm Ni. The reactor was then purged with helium, hydrogen, and a 10 mol% H_2S/H_2 mixture (100 cc/min, each for 30 min), pressurized to 1500 psi, and heated to 320°C over a period of about 3 h. Once the reactor had reached steady-state conditions, Ni-EP concentrations were monitored by periodic sampling over the duration of the batch experiments, which was approximately 25 h. Each batch experiment resulted in the deposition of approximately 3.4–4.0 wt% Ni on the microporous γ-Al_2O_3, as calculated by a Ni material balance. In the first batch experiment, however, the starting Ni-EP concentration was 68 ppm Ni, and the deposited metal was approximately 0.7 wt% Ni. At the conclusion of the series of eight experiments the reactor was disassembled, and the alumina samples were quickly transferred to an inert-atmosphere glove box, where they were cleaned and stored prior to analysis.

TABLE 2

Summary of Analytical Techniques Used

Sample no.	Treatment	TEM	XPS
1	Fresh	Fig. 2	
2	Aged	Fig. 3	
3	Fresh	Fig. 4	Ref (*6*)
4	Aged	Figs. 5–8	Figs. 9 and 10

3. ANALYTICAL TECHNIQUES

Table 2 summarizes the analytical techniques used on aged and fresh samples considered in this study as well as those used by us (*6*) earlier. Two techniques were used for the analysis of aged and fresh films, namely TEM and X-ray Photoelectron Spectroscopy (XPS). Each method requires different sample preparation techniques, which are briefly summarized below.

TEM

Various techniques have been developed and used to examine surface films of Al in TEM. Replicas and stripped films enable assessment of the topography and morphology from a plan view (*14*), while replicas of fractured sections have been used extensively to study cross-sectional structures (*15, 16*). The application of ultramicrotomy to the electron optical examination of the surface films of Al has been reported by several investigators (*17, 18*). The model alumina support, Sample 4 was ultramicrotomed to give a cross-sectional view of the pores using the method described by Furneaux *et al.* (*17*). The procedure used to obtain a ultramicrotomed section of the microporous γ-Al_2O_3 alumina support, Sample 2 is reported in (*13*).

XPS

Sample 4 was affixed to a sample button using conductive silver paint and introduced into the ESCALAB (I) surface analysis instrument. This instrument operates under ultrahigh vacuum (UHV) conditions; in this case the operating pressure was approximately 5×10^{-9} torr. XPS data were collected using nonmonochromatic Mg$K\alpha$ (1253.6 eV) radiation from a dual anode X-ray source operating at 14 kV, 20 mA. The photoelectrons were collected at an angle normal to the plane of the surface. A survey scan and elemental scans for the $C_{1s_{1/2}}$, $Al_{2p_{3/2}}$, $Al_{2p_{1/2}}$, $S_{2p_{3/2}}$, $S_{2p_{1/2}}$, O_{1s}, and $Ni_{2p_{3/2}}$ regions were collected. After analysis, the sample was etched using a large-spot argon ion gun operating at 5 kV, 65 μA for gradually increasing duration.

All the data were analyzed to find the peak areas and positions; these values are not reported here for the sake of brevity. The peak areas were subsequently corrected for instrumental and theoretical variations using sensitivity factors. Peak positions were corrected for charging effects by referencing to the $Al_{2p_{3/2}}$, $Al_{2p_{1/2}}$ peaks at 74.6 eV.

4. RESULTS AND DISCUSSION

TEM

The TEM analysis of the fresh and aged microporous γ-Al_2O_3 has been described fully by Smith and Wei (*5*). Figure 2 shows a TEM micrograph of Sample 1, the low-promoter γ-Al_2O_3 substrate, which was used for comparative studies. This sample has not been sulfided, and has not been subjected to hydrodemetallation. Needle-like alumina platelets of an approximate diameter of 30 Å and lengths up to 500 Å, in random orientation often overlapping, are the main features of this micrograph. Pores resulting from a random stacking of these platelets would therefore have random shapes and are impossible to identify in this micrograph.

Figure 3 is a TEM micrograph of Sample 2, the low-promoter γ-Al_2O_3 carrier loaded to about 25 wt% Ni due to Ni-EP hydrodemetallation. Comparison of Fig. 3 with Fig. 2 shows that the presence of Ni sulfide at this loading introduces a new feature to the TEM micrograph, namely dark spots, which are spatially dispersed Ni_3S_2 crystallites. The characteristic average dimension of the crystallites in Fig. 3 is estimated to be 250 Å. Given the average pore diameter of 85 Å (see Table 1), it is inevitable that crystallite growth is not bound by the size of the pores. No specific orientational relationship between the alumina platelets and the crystallites is readily apparent. Crystallite overlap is frequent and no universal crystal shape can be identified. Assuming a sample thickness of 70 nm, the number of crystallites per unit volume is estimated as 5×10^{-6} crystals/nm^3. When multiplied with the observed crystallite diameter this value yields a total metal loading of about 12 wt% Ni or 55% of the bulk measured value, good agreement given the uncertainties involved in making the TEM estimates. The observation corresponds to approximately 80,000 nm^2 of alumina surface area per Ni_3S_2 crystallite.

Figure 4 shows a TEM micrograph of the microtomed section of Sample 3. The Al metal and the porous oxide layer are easily distinguished in this micrograph. The metal being the dense region extending the lower part of the micrograph and the porous oxide layer on top of the metal, extending the width of the micrograph. Some damage seems to have resulted from microtoming in the form of fragmentation of the oxide layer, but the oxide layer seems to have retained its idealized form shown in Fig. 1. The oxide layer thickness can be measured from this micrograph to be 1.5 μm. The region above the porous oxide layer consisting of the embedding material, used in the microtoming process, seems to have adhered to the porous oxide layer reasonably well, but seems to have penetrated the pores to a very limited depth if at all.

Figure 5 is a low magnification TEM micrograph of Sample 4. The existence of a

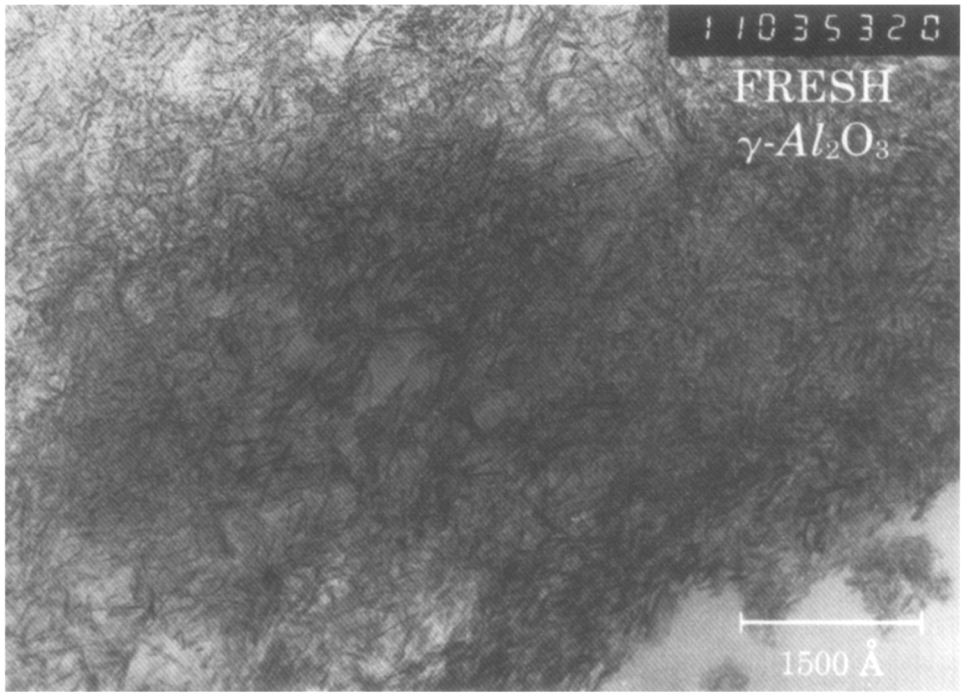

FIG. 2. TEM micrograph of Sample 1 (fresh γ-Al_2O_3)

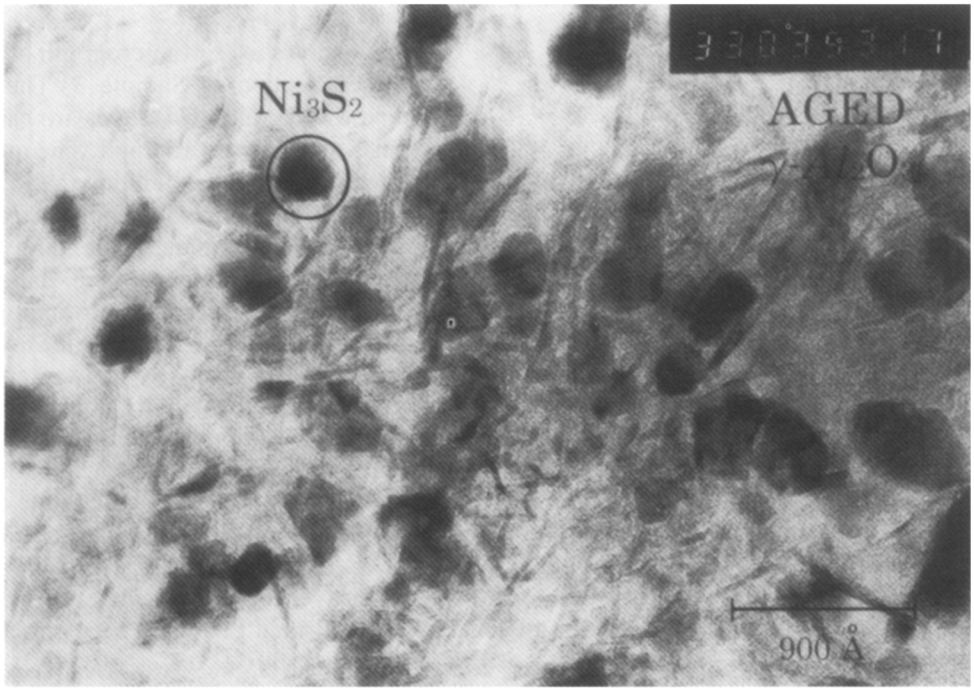

FIG. 3. TEM micrograph os Sample 2 (aged γ-Al_2O_3).

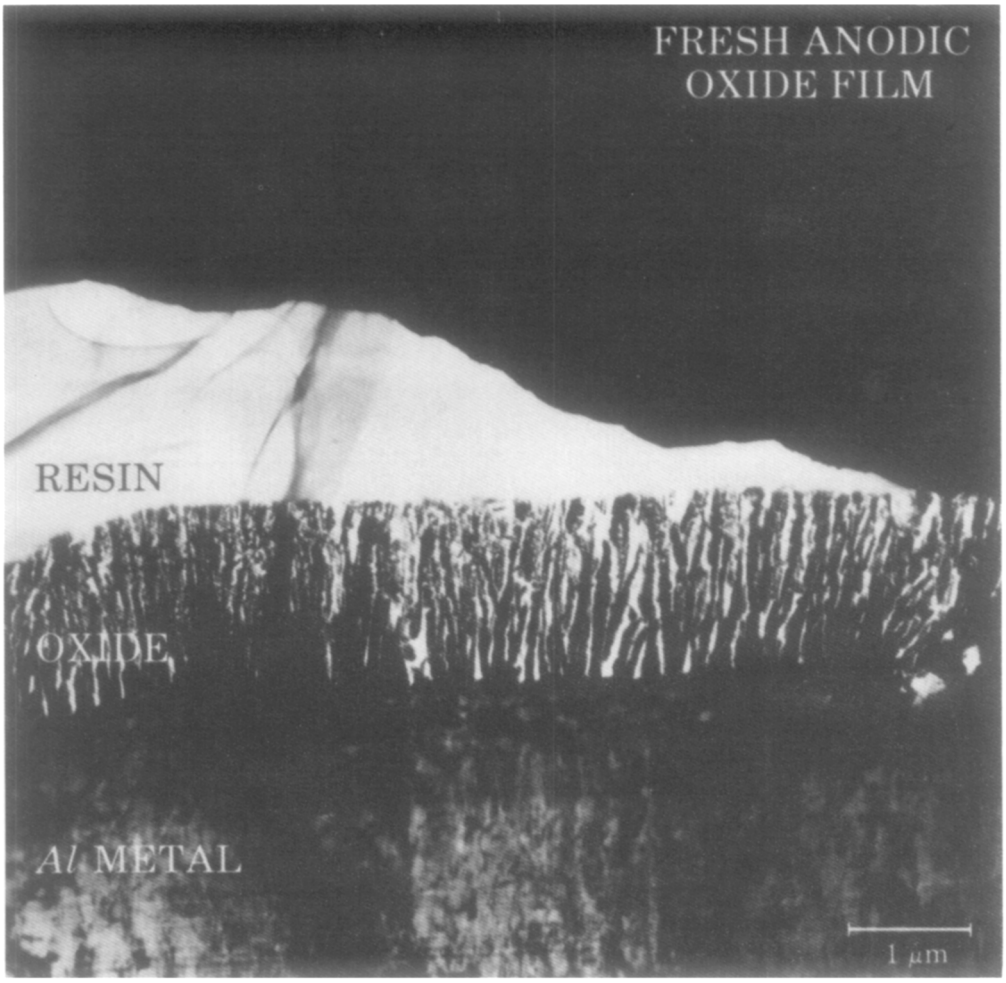

FIG. 4. TEM micrograph of Sample 3 (fresh anodic alumina film).

relatively thick layer of ca. 0.1–0.2 μm on the exposed surface of the film is clearly evident. This layer is clearly absent in Sample 3 shown in Fig. 4 and is believed to be primarily of carbonaceous nature. This relatively thin layer has adhered in some parts to the embedding material and has subsequently separated during the microtoming process in some regions. Closer examination of the film further removed from the surface of the oxide film shows some regions of high electron transparency separated by regions of dense material believed to result from wrinkling, which may have occurred during microtoming.

Figure 6 is the higher magnification micrograph of the bulk region of Sample 4. The dominant feature in this micrograph is a large number of regularly shaped crystallites distributed throughout the film. About 180 crystallites were identified in an area of 1.42×10^6 nm^2 (944 nm $\times$ 1500 nm) in the lower left-hand side of Fig. 6. Assuming a sample thickness of 100 nm gives 1.3×10^{-6} crystallite/nm^3 as compared to a value of 5×10^{-6} crystallite/nm^3 calculated for Sample 2. Using the values of specific surface area and bulk density listed in Table 1 gives 7,000 nm^2/crystallite for Sample 4, as compared to 80,000 nm^2/crystallite for Sample 2.

FIG. 5. TEM micrograph of Sample 4 (aged anodic alumina film).

Figure 7 is high magnification TEM micrograph of Sample 4. This micrograph depicts the area at the bottom of a pore. Material of different thickness appears with different brightness. Material comprising the pore wall appears darkest, while the area comprising the pore space appear brightest. The circular section of the hemispherical barrier layer separating the metal and the bulk porous oxide is clearly visible in the lower left hand side of the micrograph. The cell size can be accurately measured in this micrograph to be ca. 1700 Å. Considering the fact that the pore has been sheared in a direction perpendicular to the walls, this seems to have brought the walls closer together particularly at distant locations from the metal/oxide interface. The pore diameter measured at the lowest region of the pore is 840 Å. It is unclear whether the fact that the pore diameter falls short of 1000 Å previously reported (*6*) is due to the truncated nature of the porous films formed in H_3PO_4 electrolyte or whether it is due to large variations in pore dimensions measured from film sections resulting from irregular fractures reported by O'Sullivan and Wood (*16*). Virtually no crystal overlap is observed, indicative perhaps of the high degree of orientation existing between the crystals and

FIG. 6. TEM micrograph of Sample 4 (aged anodic alumina film) at higher magnification.

the pore wall. Crystal/oxide overlap is, however, apparent in several instances (crystallite D). Most importantly the crystals are physically attached to the pore wall (see crystallites A, B, C, E, F, G, H, and J), extending into the pore space. Less emphasis can be placed on the distance between crystals, since crystals could have potentially been displaced from their original positions relative to the pore wall (see crystallite I). The distance between crystallites A and B in Fig. 7, which seem to have remained attached to the pore wall, is 1100 Å.

For the purpose of an even closer visual examination of these features, it was found instructive to optically magnify regions of the micrograph shown in Fig. 6. This magnification is depicted in Fig. 8. A total of ca. 50 crystallites were identified in this figure and their size was determined. The crystal size was taken to be the largest dimension of the crystal that could be identified. The distribution was found to be normal with an average crystal size of 250 Å. Crystallite geometry is remarkably uniform. In many instances crystallites appear completely detached and isolated from the anodic alumina substrate. This can give much clearer insight

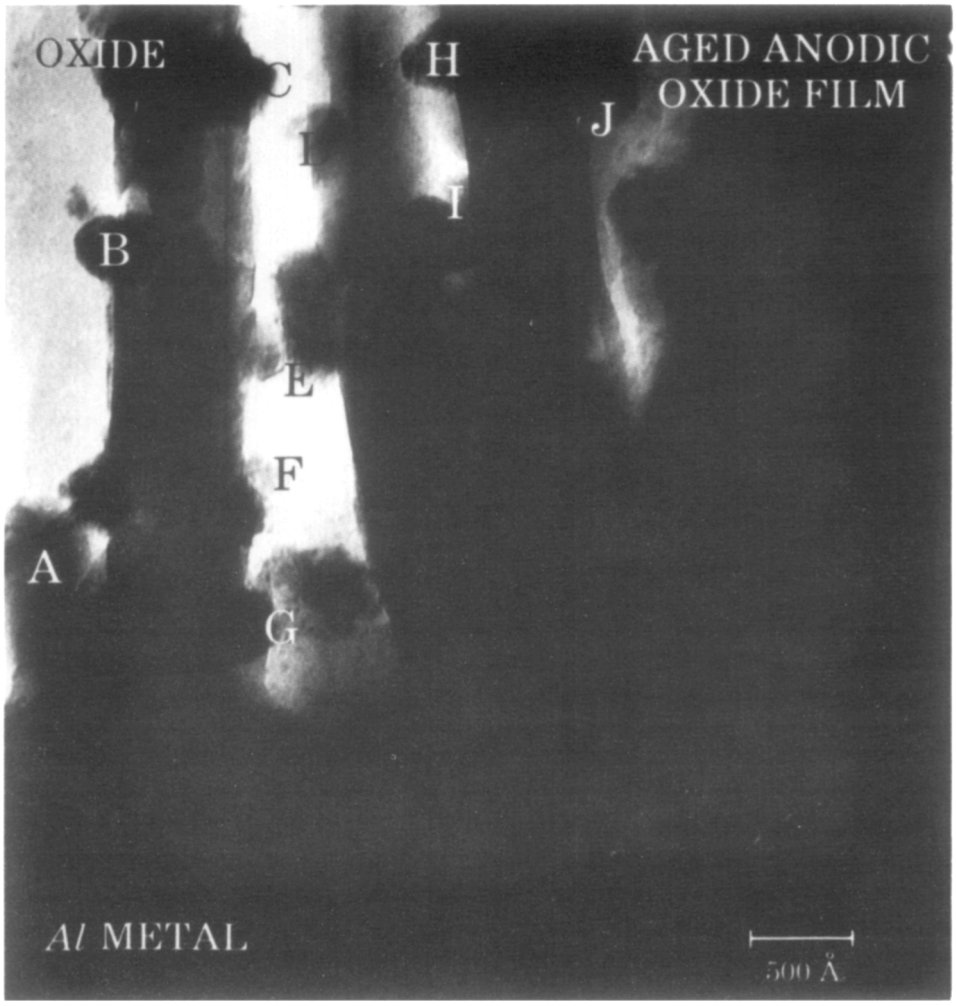

FIG. 7. High magnification TEM micrograph of the cross section of a single pore in sample 4 (aged anodic alumina film).

into the crystallite shape and any possible preferred direction of growth as compared to the Sample 2, shown in Fig. 3, in which crystallites overlap regularly and often overgrow the pores present in the γ-Al_2O_3 substrate.

XPS

Etching of Sample 4 caused the gradual removal of the alumina film. No data are available to estimate the relative etching rates of the films constituent's elements. However, it is expected on the basis of atomic weight values that the etching rate should roughly follow the trends C, O < Al, S < Ni. Bearing this in mind, C, Al_{metal}/Al_{oxide}, S, and Ni species concentration plotted as a function of etch-time are shown in Fig. 9.

Figure 9a shows that the C concentration as a function of etch-time. The sharp drop in the concentration of carbonaceous deposits as a function of etch-time supports the earlier observation of a relatively dense layer (ca. 0.1–0.2 μm thick) believed to be primarily carbonaceous on the exterior of

FIG. 8. Optical magnification of a region shown in Fig. 6.

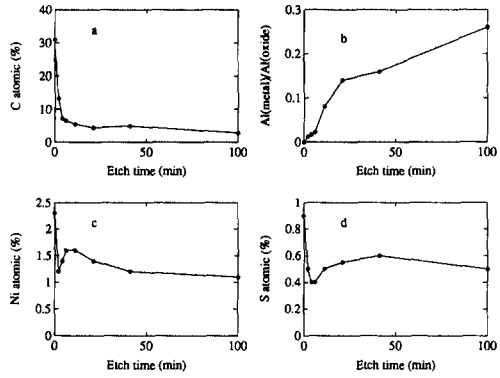

FIG. 9. Depth profiling of Sample 4 (aged anodic alumina film) using XPS.

Sample 4. This is also in accord with the fact that coking in hydrotreating catalysts starts at the exterior of the catalyst particle (*19–21*).

Figure 9b shows the ratio of Al present in metallic to the Al present in the oxide form as a function of etch-time. A gradual increase in metallic Al levels corresponds to the uncovering of Al substrate.

Figure 9c shows the Ni concentration as function of etch-time on a C free basis. A sharp drop-off at the beginning of etching corresponds to a decrease in concentration of Ni species at the very surface of the original film. Beyond the initial sharp drop in Ni concentration, which is believed to be representative of the carbonaceous overlayer, the gradual increase and the subsequent decrease in Ni concentration as a function of etching time probably reflects a similar general trend in Ni profile within the film. The film surface Ni species are predominantly trivalent oxides and the film bulk Ni species univalent, as is evidenced by an examination of $Ni_{2p_{3/2}}$ spectrum before and after etching shown in Fig. 10. This hypothesis is supported by the satellite structure (higher BE shoulder) in the $Ni_{2p_{3/2}}$ spectra before etching, as well as the $Ni_{2p_{3/2}}$ peak position.

Figure 9d shows the S concentration as function of etch-time on a C free basis. A trend similar to that observed in Ni profile is evident here, though beyond the initial sharp drop, the gradual increase and the subsequent decrease are less pronounced than that observed in Ni profile. Further evidence of extensive surface oxidation was observed in the S speciation. The $S_{2p_{3/2}}$ and $S_{2p_{1/2}}$ spectrum indicate that about half of the film's surface S species are sulfates; sulfides speciation is predominant throughout the interior of the film.

Thus a general reduction trend appears to accompany the etching procedure. Whether this evidence of reduction reflects the actual chemical speciation through the film or is a by-product of the etching process itself is impossible to determine from these data.

O, P levels on a C free remained relatively constant at ca. 63 atomic % and 3 atomic %, respectively.

5. CONCLUSIONS

Our major conclusions from our studies using porous anodic alumina films in a model hydrodemetallation experiment are:

1. Metal deposition was studied in porous anodic alumina films. TEM showed regularly shaped crystallites deposited throughout the film. The mean crystallite size was determined to be about 250 Å in two different substrates of widely varying mean pore size and structure. The number of crystallites per unit volume was found to be comparable in aged γ-Al_2O_3 and aged anodic alu-

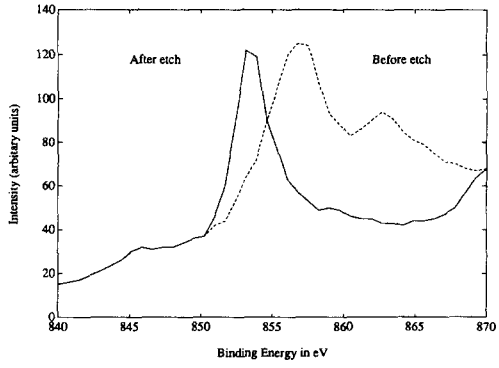

FIG. 10. $Ni_{2p_{2/2}}$ spectra before and after etching the aged anodic film.

mina films, while alumina surface area per crystallite estimated for aged γ-Al_2O_3 was 10 times higher than that in aged anodic alumina films. Crystallites were found to attach themselves to the pore wall and extend into the pore space in the case of aged anodic alumina films. A region of ca. 0.1–0.2 μm was identified at the oxide film–bulk interface and is believed to be of primarily carbonaceous nature.

2. The TEM study of aged γ-Al_2O_3 as well as that of aged anodic alumina substrates provides strong evidence in support of a nonuniform metal deposition mechanism.

3. XPS was used in conjunction with repeated Ar etching on the aged anodic alumina films. The Al_{metal}/Al_{oxide} ratio as a function of etch-time suggests that the depth profiled was only a fraction of the total oxide film thickness. The C depth profile confirms the existence of a heavy coked region at the initial surface. Repeated argon etching decreases the C concentration in this region considerably. Ni and S concentrations as a function of etch-time were obtained using XPS.

Our experimental results seem to suggest (as pointed out by one of the referees) an apparent insensitivity of the Ni deposition reaction to the pore structure and surface area of the two aluminas used in this study, whose surface texture, type of sites, and promoters are expected to be quite different. Without further experiments aimed specifically at resolving this issue it would be speculative for us to make any firm statements, at this point, as to why this might be the case or to elaborate on the implications of this behavior on the HDM reaction mechanism.

ACKNOWLEDGMENTS

This work results from a collaborative research effort between the UNOCAL Science and Technology Division and the Chemical Engineering Departments at the University of Southern California and Massachusetts Institute of Technology. I.A.W. thanks the UNOCAL Corporation for the opportunity to participate in this effort. I.A.W., N.N., and T.T.T. acknowledge partial support for this work from the US Department of Energy. They also thank Mr. P. McCaslin of Unocal Science & Technology for the XPS work and Mr. J. Brown of the Energy and Materials Science Laboratory of the Georgia Tech Research Institute of the Georgia Institute of Technology for the TEM work. Erja Rautiainen of Neste Oy Company, Finland assisted with the HDM experiments.

REFERENCES

1. Sie, S. T., *in* "Catalyst Deactivation" (B. Delmon and G. F. Froment, Eds.), Vol. 6, p. 545. Elsevier, Amsterdam, 1980.
2. Takeuchi, C., Asaoka S., Nakata, S., and Shiroto, Y., *ACS Reprints, Div. Petrol. Chem.* **30,** 96 (1985).
3. Silbernagel, B. J., *J. Catal.* **56,** 315 (1979).
4. Toulhoat, H., Plumail, J. C., Houpert, C., Szymanski, R., Bourseau, P., and Muratet G., *ACS Preprints, Div. Petrol. Chem.* **32,** 463 (1987).
5. Smith, B. J., and Wei, J., submitted for publication.
6. Nourbakhsh, N., Tsotsis, T. T., and Webster, I. A., *Appl. Catal.* **50,** 65 (1989).
7. Cocke, D. L., Johnson, E. D., and Merrill, R. P., *Catal. Rev. Sci. Eng.* **26,** 163 (1984).
8. Agrawal, R., and Wei, J., *Ind. Eng. Chem. Process Des. Dev.* **23,** 505, 515 (1984).
9. Hung, C. W., and Wei, J., *Ind. Eng. Chem. Process Des. Dev.* **19,** 250, 257 (1980).
10. Ware, R. A., and Wei, J., *J. Catal.* **93,** 100, 122, 135 (1985).
11. Webster, I. A., and Wei, J., *ACS Reprints, Div. Petrol. Chem.* **30,** 37 (1985).
12. Limbach, K. W., Ph.D. thesis, Massachusetts Institute of Technology, 1989.
13. Smith, B. J., Ph.D. thesis, Massachusetts Institute of Technology, 1988.
14. Chu, Y. F., and Ruckenstein, E., *Catal. Rev. Sci. Eng.* **41,** 384 (1976).
15. Booker, C. J. L., Wood, J. L., and Walsh, A., *Brit. J. Appl. Phys.* **8,** 347 (1957).
16. O'Sullivan, J. P., and Wood, G. C., *Proc. Roy, Soc. London A* **317,** 511 (1970).
17. Furneaux, R. C., Thompson, G. E., and Wood, G. C., *Corros. Sci.* **18,** 481 (1978).
18. Xu, Y., Thompson, G. E., and Wood, G. C., *Electrochim Acta* **27,** 1623 (1982).
19. Ohtsuka, T., *Catal. Rev. Sci. Eng.* **16,** 291 (1977).
20. Tamm, P. W., Harnsberger, H. F., and Bridge, A. G., *Ind. Eng. Chem. Process Des. Dev.* **20,** 262 (1981).
21. Stanulonis, J. J., Gates, B. C. and Olson, J. H., *AIChE J.* **22,** 576 (1976).